Research Article

Journal of RAMAN SPECTROSCOPY

Received: 21 April 2010 Accepted: 28 July 2010 Published online in Wiley Online Library: 27 September 2010

(wileyonlinelibrary.com) DOI 10.1002/jrs.2790

A comprehensive spectroscopic study of synthetic Fe^{2+}, Fe^{3+}, Mg^{2+} and Al^{3+} copiapite by Raman, XRD, LIBS, MIR and vis–NIR

W. G. Kong,[a,b]* Alian Wang,[b] John J. Freeman[b] and Pablo Sobron[b]

The identification of iron sulfates on Mars by the Mars Exploration Rovers (MERs) and the Mars Reconnaissance Orbiter emphasized the importance of studying iron sulfates in laboratory simulation experiments. The copiapite group of minerals was suggested as one of the potential iron sulfates occurring on the surface and subsurface on Mars, so it is meaningful to study their spectroscopic features, especially the spectral changes caused by cation substitutions. Four copiapite samples with cation substitutions (Fe^{3+}, Al^{3+}, Fe^{2+}, Mg^{2+}) were synthesized in our laboratory. Their identities were confirmed by powder X-ray diffraction (XRD). Spectroscopic characterizations by Raman, mid-IR, vis-NIR and laser-induced-breakdown spectroscopy (LIBS) were conducted on those synthetic copiapite samples, as these technologies are being (and will be) used in current (and future) missions to Mars. We have found a systematic ν_1 peak shift in the Raman spectra of the copiapite samples with cation substitutions, a consistent atomic ratio detection by LIBS, a set of systematic XRD line shifts representing structural change caused by the cation substitutions and a weakening of selection rules in mid-IR spectra caused by the low site symmetry of $(SO_4)^{2-}$ in the copiapite structures. The near-infrared (NIR) spectra of the trivalent copiapite species show two strong diagnostic water features near 1.4 and 1.9 μm, with two additional bands near 2.0 μm. In the vis-NIR spectra, the position of an electronic band shifts from 0.85 μm for ferricopiapite to 0.866 μm for copiapite, and this shift suggests the appearance of a Fe^{2+} electronic transition band near 0.9 μm. **Copyright © 2010 John Wiley & Sons, Ltd.**

Keywords: Raman spectroscopy; Mars; iron sulfates; copiapite; cation substitutions

Introduction

The copiapite group of minerals is frequently observed as precipitation and evaporation products in terrestrial acidic mine drainage sites. Various members of this group of minerals were identified in Rio Tinto region, Spain,[1–3] in a coal mine in Pennsylvania[4] and in Iron Mountain, California.[5,6] Copiapite minerals with variety of cation substitutions are frequently found in the nature. The end members of copiapite-group minerals found in Rio Tinto region are aluminocopiapite, magnesiocopiapite, cuprocopiapite, ferricopiapite and copiapite, while those found in the Iron Mountain area are mostly magnesiocopiapite and aluminocopiapite.

Sulfates have been found on Mars by spectrometers on orbiters (OMEGA on Mars Express and CRISM on Mars Reconnaissance Orbiter) and by spectrometers on two Mars Exploration Rovers (MERs) (Pancam, MiniTES, Alpha particle X-ray spectrometer (APXS) and Mössbauer (MB) spectrometer). The orbital remote sensing observed wide distributions and large quantities of Mg and Ca sulfates on Mars.[7–19] Iron sulfates have also been detected at localized areas.[11,20–22] Iron sulfates were identified at two MER exploration sites.[23–26] Jarosite [$(K,Na,H_3O)Fe_3(SO_4)_2(OH)_6$] was identified by the MB spectrometer on the Opportunity rover.[27] The mineral modal analysis based on APXS and MB data suggests that the jarosite abundance is just over 10 wt% of Meridiani outcrop.[28] A nonspecific ferric sulfate is indicated by the MB spectral analysis of the light-toned salty soils exposed by Spirit rover at several sites (Paso Robles, Dead Sea and Tyrone) in Columbia Hills at the Gusev Crater.[29–36] Ferricopiapite, hydronium jarosite, fibroferrite, rhomboclase and paracoquimbite are suggested by a study using the deconvolution of Pancam spectra.[37] Ferricopiapite has also been suggested as the major sulfur-bearing constituent in Paso Robles salty soils by a study combining the Pancam, MB and MiniTES data from Spirit with laboratory experiments.[38] Ferricopiapite, fibroferrite and paracoquimbite are suggested by the spectral unmixing of Pancam images of soils in the Gusev crater.[39] These findings and investigations reinforce the importance of obtaining a better understanding of spectroscopic properties of the copiapite group of minerals through laboratory experiments.

Copiapite-group minerals with cation substitutions have been investigated by mid-IR and vis–NIR spectroscopy (Majzlan and Bishop). Raman spectra with sharper peaks may show more subtle spectral differences among these copiapite-group minerals, and these differences may help us in future Mars expolorations to distinguish between different copiapite minerals. Our study was also designed to provide reference spectra for analyzing data obtained from current and future missions to Mars. Four cations (Fe^{3+}, Fe^{2+}, Mg^{2+}, Al^{3+}) were used for synthesizing four minerals of

* *Correspondence to: W. G. Kong, School of Physics, Shandong University, Jinan 250100, China. E-mail: gavink@levee.wustl.edu*

a *School of Physics, Shandong University, Jinan 250100, China*

b *Department of Earth and Planetary Sciences and McDonnell Center for Space Sciences, Washington University, St. Louis, MO 63130, USA*

Copyright © 2010 John Wiley & Sons, Ltd.

Journal of RAMAN SPECTROSCOPY

the copiapite group: ferricopiapite, copiapite, magnesiocopiapite and aluminocopiapite. Their structures were confirmed by powder X-ray diffraction (XRD) analysis. Spectroscopic investigations using Raman, mid-IR, vis–NIR and LIBS were undertaken to generate the reference spectra needed for the analysis of the data obtained from both orbital and landed mission observations.

Synthesis and Measurements

Preparations of samples

The following chemicals were used to synthesize the minerals: ferric sulfate pentahydrate ($Fe_2(SO_4)_3 \cdot 5H_2O$, 97%, Acros Organics), ferrous sulfate heptahydrate ($FeSO_4 \cdot 7H_2O$, 99.5%, Acros Organics), magnesium sulfate monohydrate ($MgSO_4 \cdot H_2O$, 97%, Sigma Aldrich) and aluminum sulfate octadecahydrate ($Al_2(SO_4)_3 \cdot 18H_2O$, 98% Acros Organics). Impurities in these chemicals arise from the same sulfate with different hydration states (e.g. the chemical $MgSO_4 \cdot H_2O$ may have 3 wt% $MgSO_4 \cdot 5H_2O$). Deionized water was used in the preparation of the aqueous solutions and distilled water was used to dilute sulfuric acid from reagent-grade H_2SO_4 obtained from Thermo Scientific.

The synthesis methods were based on the reports by Friedlander and Majzlan.[40,41] Supersaturated aqueous solutions were prepared by mixing the required reagents with diluted H_2SO_4 that controls the pH values. The pH value of the solution was measured using a pH meter with a resolution of 0.1 pH units. The starting solutions were placed in an oven maintained at 50 °C.

After several days, ferricopiapite, copiapite, magnesiocopiapite and aluminocopiapite precipitated from the solutions as fine crystals with a grain size of 1–80 μm. The products were repeatedly washed with ethanol and then dried in air.

The hydration impurities of the starting sulfates account for no more than 1 wt% sulfates other than copiapite products and do not have significant influence on this spectroscopic study due to their low level of abundance. In the synthesis process, one reagent was completely dissolved before another was added. An ultrasonic bath was used to dissolve the chemicals. One hundred Raman spectra were obtained on each copiapite sample to check the homogeneity. A sample was used for spectroscopic studies only when no differences were observed among the 100 Raman spectra of that sample.

X-ray diffraction measurements

Powder XRD measurements were carried out with a Rigaku Geigerflex D-MAX/A diffractometer with a Cu Ka X-ray source. The instrument is equipped with a vertical goniometer and a scintillation counter. The XRD patterns of the samples were collected at a 2θ range of 3–50° with a step size of 0.04° and a dwell time of 1 s. The peak positions were calibrated using the Si(111) spacing of a standard Si reference powder obtained from the National Bureau of Standards (NBS, now the National Institute of Standards and Technology (NIST)). This standard provided an accuracy of 0.001° in 2θ. The Jade software (Sept. 2009 version) database was used to analyze the XRD data.

LIBS spectral measurements

LIBS spectra from the four copiapite samples were collected at the LIBS lab at Washington University. The fine crystalline copiapite samples were pressed into pellets of about 2 cm in diameter using a pressure of 10 t. A Nd : YAG laser (Minilite-II by Continuum) was used to generate high-intensity laser pulses at the wavelength of 1064 nm delivering 40 mJ per pulse at the sample surface with 7-ns duration at 10-Hz repetition rate. The emission from the atoms and ions in the plasma was collected by an uncoated UV-enhanced optical fiber placed at about 10 mm away from the sampling surface and at 45° from the laser beam. The collected photons were dispersed by an Echelle spectrograph (Andor Mechelle ME5000) and detected by an intensified charge coupled device (CCD) camera (Andor iStar DH 720-25U-03). The camera gating was synchronized with the laser pulse generation. LIBS spectra were recorded in the 300–900 nm wavelength range with a maximum resolution of 0.05 nm at 300 nm. The spectrograph and the detector were wavelength-calibrated using ten lines from an NIST-traceable Hg/Ar lamp. In order to correct for the nonlinear efficiency of the dispersion grating, an NIST-traceable dual deuterium/quartz tungsten halogen lamp was used as an instensity standard for calibrating the detector's spectral response.

Raman spectral measurements

Raman spectra were collected with a HoloLab5000-532 laser Raman spectrometer (Kaiser Optical Systems Inc. (KOSI)), using the 532-nm line of a frequency-doubled, CW Nd : YAG laser as the excitation source. The spectrometer covers a Raman spectral range of 4000–100 cm^{-1} with a spectral resolution of 4–5 cm^{-1}. A 20× microscope objective (0.4 NA) with a working distance of 1 cm was used for these measurements. This objective produces a condensed laser beam of 6 μm diameter at the focus. The wavelength calibration of the Raman spectrometer was carried out using a neon emission lamp. The spectral intensity was corrected against a secondary intensity standard tungsten lamp calibrated at KOSI. The laser wavelength was checked on each working day using the Raman peak of a Si wafer at 520.7 cm^{-1} at 20 °C, and was corrected to be within ±0.2 cm^{-1}. The wavelength accuracy and precision were found to be better than 0.1 cm^{-1} in the spectral region of interest as determined by the spectral peak fitting using the GRAMS-32 AI software.

Mid-IR spectral measurements

The mid-IR spectra were collected using a ThermoNicolet Nexus 670 Fourier transform infrared (FTIR) spectrometer (Thermo Fisher Scientific Inc.). It has an ETC EverGlo IR Source, and the attenuated total reflectance (ATR) spectra were obtained using a Harrick 'Golden Gate' diamond anvil ATR unit. The spectrometer was set to collect data from 400 to 4000 cm^{-1} with spectral resolution of 4 cm^{-1}. The ATR measurements were made by pressing a few grains of sample on the diamond anvil of the Golden-gate ATR unit.

Vis–NIR spectral measurements

An Analytical Spectral Device (ASD) made by ASD Inc. covering a spectral range of 400–2500 nm was used to acquire vis–NIR reflectance spectra of our samples. The spectra were collected simultaneously in three spectral ranges: visible (vis) (350–1000 nm), shortwave near-infrared (NIR) (1000–1700 nm) and NIR (1700–2500 nm). The spectral resolution (full-width at half-maximum, FWHM) is 3 nm for the region 350–1000 nm and 10 nm for the region 1000–2500 nm. The wavelength of this device is calibrated by ASD Inc. annually using atomic emission lines

 Copyright © 2010 John Wiley & Sons, Ltd.

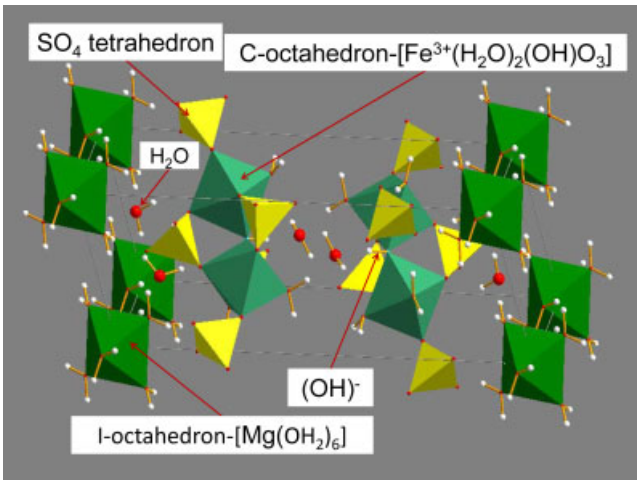

Figure 1. Magnesiocopiapite [$MgFe_4^{3+}$ $(SO_4)_6(OH)_2 \cdot 20H_2O$] crystal structure based on the data reported by Majzlan and Kiefer.[42] The cation substitutions occur at the I octahedral sites.

from a low-pressure gas emission lamp. A lamp and power supply from Optronic Laboratories Inc., which is traceable to NIST, was used by ASD Inc. to make intensity calibration for this device. The instrument was optimized using the software provided by ASD Inc. A diffuse white light reference plate provided by ASD Inc. was used as the white 100% reflectance standard. Reflectance spectra were obtained directly from powder copiapite samples placed in an aluminum sample holder with a well 2 cm in diameter and 5 mm deep. Each spectrum was averaged over 50 scans.

Structure, Vibrational Mode Analysis and Electronic Transitions

The crystal structure of copiapite

The crystal structure data used in this study are from the study by Majzlan and Kiefer[42] for ferricopiapite and magnesiocopiapite and by Fanfani *et al.*[43] for copiapite. A general formula [$I_{1or2/3}Fe_4^{3+}$ $(SO_4)_6(OH)_2 \cdot 20H_2O$] can be used to represent the four synthetic copiapite samples in this study, where I = Fe^{3+}, Fe^{2+}, Mg^{2+}, Al^{3+}. In the structure of copiapite (Fig. 1), there are three crystallographically distinct $(SO_4)^{2-}$ tetrahedra and two different types of octahedra (called I and C in this study). The sulfate tetrahedra connect the C octahedra [Fe^{3+} $(O\ H_2)_2(OH)O_3$] by sharing O^{2-} to form infinite chains. The two nearby C octahedra are directly connected by sharing $(OH)^-$. The I octahedra ([$I_{1or2/3}(OH_2)_6$]) are isolated and occupy the space between the sheets formed by these infinite chains. There are six water molecules per formula which do not directly connect with cations to form octahedra but are weakly linked to octahedra and tetrahedra through hydrogen bonding. For magnesiocopiapite and copiapite, I sites are completely filled by divalent cations. For ferricopiapite and aluminocopiapite, only two-thirds of the I sites are filled with trivalent cations.

Fundamental vibrational modes in Raman and mid-IR spectra

Copiapite-group minerals have low structural symmetry. All four studied copiapites belong to space group P_i (C_i). We conducted the vibrational mode analysis using group theory and a correlation method,[44] and found the fundamental vibrational modes of copiapite-group minerals to be

$$\begin{aligned}\Gamma^{\text{crystal total}} &= \Gamma^{SO4} + \Gamma^{(OH)} + \Gamma^{H2O} + \Gamma^{Fe} - \Gamma^{\text{acous}} \\ &= (45A_g + 45A_u)^{SO4} + (6A_g + 6A_u)^{(OH)} + (90A_g + 90A_u)^{H2O} \\ &\quad + (6A_g + 9A_u)^{Fe} - (3A_u)^{\text{acous}} = 147A_g(\text{R}) + 147A_u(\text{IR}) \qquad (1)\end{aligned}$$

There is one molecule in the unit cell for copiapite-group minerals. Group theory analysis showed that copiapite structures have 294 fundamental vibration modes, where 147 A_g modes are Raman active and 147 A_u modes are IR active. Among the Raman active vibrational modes A_g, 45 modes are from SO_4 tetrahedra, 6 modes are from $(OH)^-$, 90 modes are from structural H_2O and 6 modes from Fe translations. The classification of A_u is very similar to that of A_g except for the appearance of three A_u acoustic modes. These acoustic modes correspond to the translational motions of the entire copiapite crystal lattices. In general, not all vibrational modes can be distinguished in the recorded Raman and mid-IR spectra. Normally, the chemical bonds with high covalency constitute the most intense peaks in Raman and mid-IR spectra (e.g. S–O bonds in copiapite). Thus the strongest Raman and mid-IR peaks in copiapite spectra are due to the fundamental vibrational modes of $(SO_4)^{2-}$, H_2O and $(OH)^-$, as shown in Table 1.

The spectral peaks in the 900–1300 cm^{-1} spectral range (Raman and mid-IR) arise from the Raman active symmetrical (ν_1) and IR active asymmetrical (ν_3) stretching vibrational modes of $(SO_4)^{2-}$. The peaks in the 400–700 cm^{-1} region arise from the symmetrical (ν_2) and asymmetrical (ν_4) bending vibrational modes of $(SO_4)^{2-}$. The reduction in symmetry of $(SO_4)^{2-}$ from T_d (as free tetrahedron) to C_1 (site symmetry) and to C_i (crystal symmetry) removes degeneracy in these fundamental modes resulting in peak splitting in both Raman and mid-IR spectra. Three crystallographically distinct sites for six $(SO_4)^{2-}$ ionic groups per formula unit would also induce differences in peak position for these fundamental modes.

The stretching modes of the $(OH)^-$ ionic groups appear as narrow peaks in the 3000–3800 cm^{-1} spectral range. The stretching modes of H_2O molecules overlap with the overtones of the bending modes and appear as broad peaks in the 3000–3700 cm^{-1} spectral range. The fundamental bending mode of the H_2O molecule contributes a peak near 1640 cm^{-1}. These H_2O and OH peaks appear in both Raman and mid-IR spectra.

In general, the M–O bonds in sulfates (M = Ca, Mg, Fe, Al) have lower covalency than the S–O bonds. Their stretching vibrational mode peaks are at longer wavelengths (far-IR range) with weak intensities and they are not listed in Table 1 for copiapite.

Overtones, combination modes and electronic transitions in vis-NIR spectra

The spectral peaks observed in the vis–NIR spectral range (400–2500 nm) are due to four processes[45]: d–d orbital electronic transitions, charge transfer electronic transitions, electronic transitions between the top of a valence band and the bottom of the conduction band and the overtones or combination modes of fundamental vibrational modes. The NIR spectral peaks of copiapite in the 1.0–2.5 μm range are mostly due to the overtones and the combinational modes of the fundamental vibrational modes of $(SO_4)^{2-}$, $(OH)^-$ and H_2O (Table 1).

A previous vis–NIR spectroscopic study of copiapite and magnesiocopiapite suggested that the spectral peaks in the 400–1000 nm range are contributed by spin-forbidden electronic

Copyright © 2010 John Wiley & Sons, Ltd.

Journal of RAMAN SPECTROSCOPY

Table 1. Peak positions and peak shoulders of Raman, MIR and vis–NIR spectra of four copiapite minerals

	H_2O vib. modes (cm^{-1})		$(OH)^-$ vib. modes (cm^{-1})	SO_4 vib. modes (cm^{-1})						Vis–NIR peaks and shoulders (nm)	
	Stretching	Bending	Stretching	ν_1	ν_2	ν_3	ν_4	Libration modes (cm^{-1})	Other peaks (cm^{-1})	Overtone, combination modes of H_2O and $(OH)^-$	Electronic transition bands of ferric cations
Aluminocopiapite	3093 IR	1636 IR	3522 R	989 IR	452 R	1093 IR	588 IR	247 R	555 R	1454 IR	430 VIS
	3164 R	1638 R	3523 IR	989 R	476 R	1123 R	598 R	270 R	553 IR	1942 IR	*~532 VIS*
	3384 R		3566 R	1018 IR		*1138 IR*	610 IR	300 R	2428 R	2208 IR	853 IR
				1019 R		*1181 IR*	614 R				
						1210 IR	632 IR				
						1220 R	636 R				
Ferricopiapite	3163 R	1635 IR	3523 IR	987 IR	453 R	1095 IR	594 IR	245 R	553 R	1453 IR	430 VIS
	3366 R	1639 R	3522 R	990 R	478 R	1123 R	600 R	269 R	552 IR	1941 IR	*~530 VIS*
	3097 IR		3567 R	1016 IR		1137 IR	613 R	303R	2427 R	2208 IR	846 IR
				1019 R		*1178 IR*	632 R				
						1209 IR	633 IR				
						1225 R					
Magnesiocopiapite	3120 IR	1643 IR	3529 R	991 IR	476 R	1093 IR	591 IR	227 R	557 R	1451 IR	430 VIS
	3167 R	1645 R	3490 IR	995 R		1102 R	597 R	252 R	552 IR	1935 IR	*~532 VIS*
	3314 R	1695 IR		1004 R		1129 R	610 IR	270 R		2202 IR	855 IR
	3331 R			1019 R		*1133 IR*	613 R	305 R			
	3499 R					*1174 IR*	633 IR				
						1218 IR	639 R				
						1225R					
Copiapite	3116 IR	1637 IR	3525 IR	993 IR	478 R	1090 IR	594 R	243 R	554 R	1450 IR	430 VIS
	3179 R	1644 R	3527 R	996 R		1115 R	610 IR	270 R	552 IR	1940 IR	*~533 VIS*
	3349 IR			1005 R		*1138 R*	614 R	304 R		2205 IR	866 IR
				1016 IR		*1139 IR*	637 R				
				1026 R		*1180 IR*	634 IR				
						1214 IR					
						1224 R					

Shoulders are shown in italics.
R, Raman peaks or shoulders; IR, IR peaks or shoulders; VIS, visual bands and shoulders.

transition between d and d orbitals of ferric cations in the C octahedra of copiapite.[46] The magnetic coupling of linked C octahedra causes relaxation of the selection rules and this transition occurs.[47] When ferric ions are bonded into crystal structure, the five degenerate 3d orbitals of free ferric ion will interact with the electromagnetic field of the surrounding ligands in the crystal and the degeneracy will be partially or totally removed. The electronic transitions in the 400–1000 nm spectral range provide information about the ligands surrounding the ferric cation in the crystal.

Results and Discussion

XRD patterns

The XRD patterns of the four synthetic copiapite samples are shown in Fig. 2. The positions of all XRD lines of ferricopiapite and magnesiocopiapite were compared with published data,[42,48] and no extra lines were observed. Fanfani *et al*. published the structural refinement results for copiapite without showing XRD data,[43] and therefore no comparison was available for copiapite.

Among the four XRD patterns (Fig. 2), we noticed the shift of the three strongest lines in the 2θ range 5–15° (marked by three dash lines in Fig. 2). The positions of the three strongest lines are listed in Table 2. Compared to those of magnesiocopiapite, the line shifts are 0.04–0.18° 2θ for copiapite, 0.13–0.4° 2θ for ferricopiapite and 0.16–0.48° 2θ for aluminocopiapite. These systematic line shifts indicate a gradual increase of the *d* spacing caused by the cation substitutions in these copiapite structures. Trivalent cations (Fe^{3+} and Al^{3+}) have a greater influence on the structural distortion since they only fill two-thirds of the I octahedra. An additional line appears near 15.48° 2θ for the trivalent copiapite species.

Elemental composition from LIBS spectra

Figure 3 shows the LIBS spectra of four synthetic copiapite samples in a selected spectral range. This range is of particular interest, as the spectral variations due to Mg, Al and Fe are found here. Fe emission lines in the LIBS spectra (Fig. 3) are common to all four copiapite samples (e.g. the peaks indicated by the dashed lines in Fig. 3), whereas three strong Mg lines at 382.9, 393.2 and 383.8 nm are present in the magnesiocopiapite sample and two Al emission lines at 394.0 and 396.2 nm in the aluminocopiapite sample. Independent calculations of the peak areas associated with Fe, Mg and Al in the spectra confirm that the abundance of the cations in the magnesiocopiapite and aluminocopiapite

 Copyright © 2010 John Wiley & Sons, Ltd.

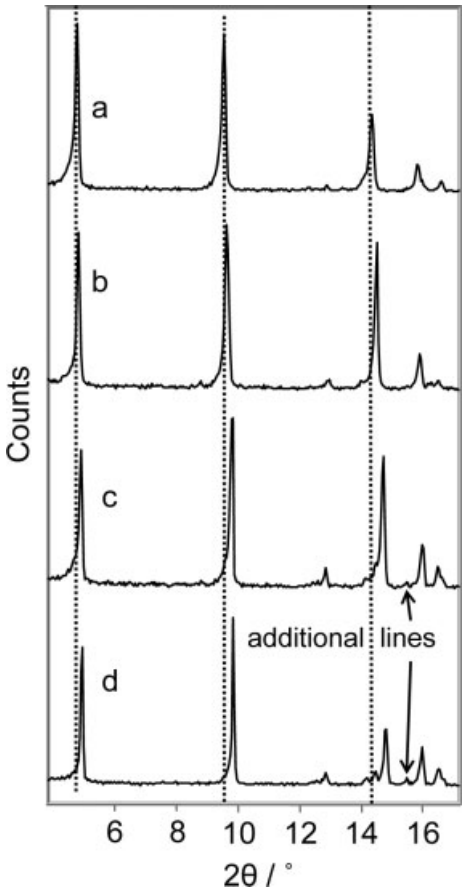

Figure 2. XRD patterns: (a) magnesiocopiapite; (b) copiapite; (c) ferricopiapite and (d) aluminocopiapite. Three dotted lines indicate the position of the three most intense XRD lines. The additional lines for trivalent copiapite samples are indicated by arrows.

Table 2. 2θ Value of three most intense XRD lines of four copiapite samples

	2θ Value (°)		
	Line 1	Line 2	Line 3
Magnesiocopiapite	4.76	9.52	14.32
Copiapite	4.8	9.6	14.48
Aluminocopiapite	4.88	9.8	14.72
Ferricopiapite	4.92	9.84	14.8

samples is consistent with the assigned chemical formulas for these two synthetic copiapite samples.

The detection and quantification of sulfur in sulfur-bearing materials by LIBS technique is very challenging under normal laboratory conditions due to the following main reasons: (1) strong S emission lines in LIBS spectra occur in the vacuum UV (<200 nm) and NIR (>900 mm) ranges,[49,50] while our LIBS system (Andor Mechelle plus Andor iStar intensified CCD) is most sensitive in the range of 200–950 nm. There are a few weak S lines that occur in the visible region (400–600 nm), but these lines overlap with Fe emission lines that are notably stronger in the plasma produced from our synthetic copiapite samples. (2) The electronically excited S in the plasma of S-bearing samples can easily react with oxygen

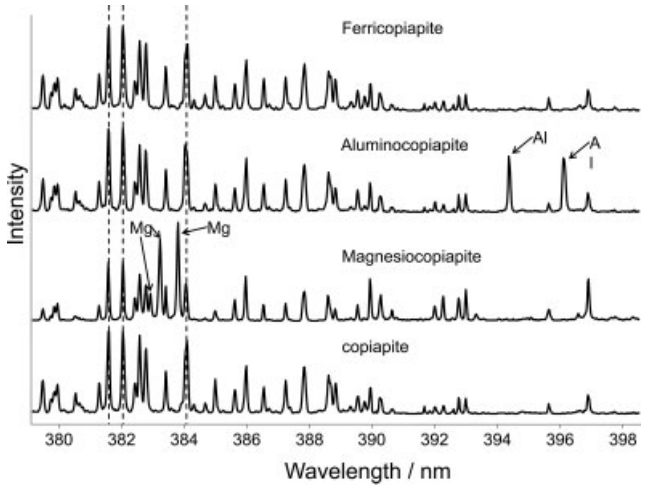

Figure 3. LIBS spectra of the four copiapite samples. The dashed lines indicate the iron emission lines for all four copiapite samples. The emission lines of Mg and Al are indicated by arrows.

in the laboratory atmosphere,[50] thereby reducing the strength of the S emission lines. In a Martian atmospheric environment (near 7 mbar CO_2), the effect of latter process does not exist, and therefore the quantification of sulfur by LIBS can be achieved.[51–54]

Changes in Raman spectral features caused by cation substitutions

Raman spectra of the four copiapite samples are shown in Fig. 4. In the 3000–3700 cm^{-1} spectral range (Fig. 4(a)), the strong and broad Raman peaks are contributed by the symmetric and asymmetric stretching modes (ν_1 and ν_3) of H_2O and the first overtone of the bending mode ($2\nu_2$). The H_2O molecules at the ten crystallographically distinct sites in copiapite[42,43] give rise to Raman peaks at slightly different wavenumbers, and these H_2O peaks overlap to form the broad band in the 3000–3700 cm^{-1} region. This overlap may be removed at lower temperature following the trend reported in the interesting studies by Chio *et al.*[55,56]

A diagnostic (sharp) Raman peak of the stretching vibrational mode of $(OH)^-$ group occurs near 3522 cm^{-1} for trivalent copiapite species and near 3528 cm^{-1} for divalent species as indicated by the dashed line in Fig. 4(a). In the Raman spectra of two trivalent copiapite species, an additional peak appears near 3566 cm^{-1} (Fig. 4(a) and Table 1). This additional peak suggests the removal of the site equivalence of two $(OH)^-$ groups in the trivalent copiapite structures.

Raman peaks and shoulders in the 400–1300 cm^{-1} spectral range were assigned, and are listed in Table 1. The Raman peaks in the 989–1026 cm^{-1} region are mainly contributed by the ν_1 vibrational mode of $(SO_4)^{2-}$ (Fig. 4(b)). Systematic peak shifts were observed, as shown in Fig. 4(b). In copiapite-group structures, there are three crystallographically distinct sites for the $(SO_4)^{2-}$ tetrahedra, and these different sites generate multiple peaks for the sulfate symmetric stretching mode. As shown in Fig. 4(b), the two sulfate ν_1 peaks appear in the 1019–1026 cm^{-1} region and in the 889–997 cm^{-1} region. An additional shoulder (~1005 cm^{-1}) occurs between the two major peaks for the divalent copiapite species. Multiple peaks were also observed for the other fundamental vibrational modes (ν_2, ν_3 and ν_4) of $(SO_4)^{2-}$ tetrahedra as indicated in Table 1.

Copyright © 2010 John Wiley & Sons, Ltd.

Journal of RAMAN SPECTROSCOPY

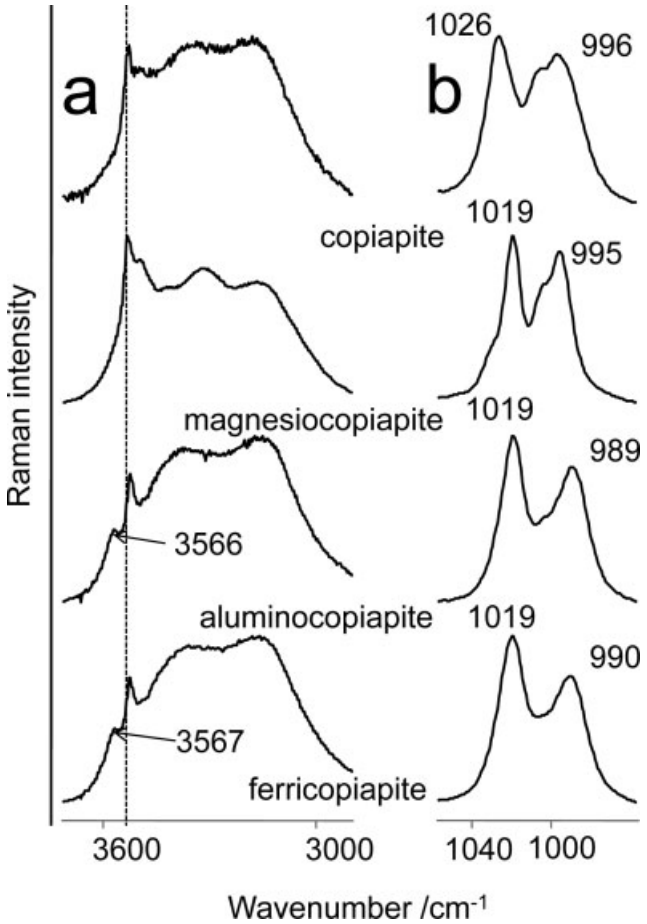

Figure 4. Raman spectra of the four copiapite samples. (a) The 3800–2800 cm^{-1} region for H_2O/OH vibrational modes. The OH peaks in the spectra of trivalent copiapite samples are indicated by arrows. (b) The 1050–900 cm^{-1} region for ν_1 symmetric mode of $(SO_4)^{2-}$ that splits into two main peaks.

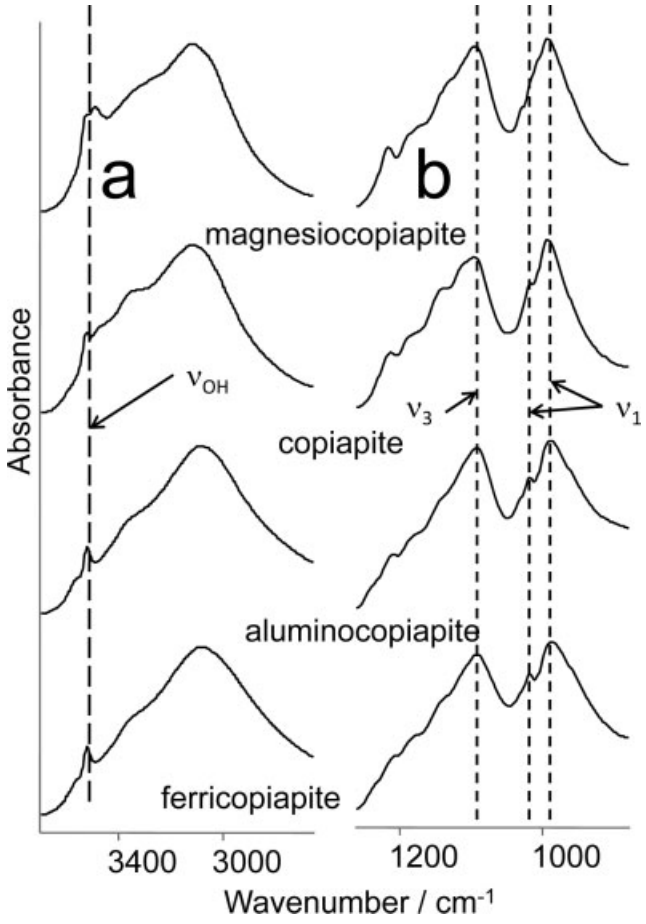

Figure 5. Mid-IR ATR spectra of the four copiapite samples. The OH stretching peaks and sulfate stretching peaks are indicated by dashed lines.

Different cations with different ionic radii, masses and charges and occupying octahedral sites give rise to variations in the structure of major covalent oxy-anionic group [$(SO_4)^{2-}$ in sulfates]. The structural changes of covalent oxy-anionic group result in shifts in the Raman peak position. By analogy, the mass effect of cation substitutions on the Raman peak positions has been reported for pyroxene,[57] olivine,[58] carbonates and sulfates,[59,60] Fe–Cr–Ti oxides[61] and feldspar.[62] Fig. 4(b) and Table 1 show that the higher wavenumber peak of the ν_1 mode of $(SO_4)^{2-}$ shifts from 1019 cm^{-1} for ferricopiapite to 1026 cm^{-1} for copiapite. Based on the crystal structure data reported by Fanfani *et al*.[43] and Majzlan and Kiefer,[42] the average S–O bonding length of $(SO_4)^{2-}$ in copiapite (1.462 Å) is smaller than that in ferricopiapite (1.478 Å). For the same element (Fe^{2+} and Fe^{3+}), a shorter bond length generally indicates a stronger bonding energy, leading to increased wavenumber of the ν_1 Raman peak. The average S–O bonding length for ferricopiapite (1.478 Å) is smaller than that in magnesiocopiapite (1.495 Å), which leads to an increased wavenumber in the Raman spectra. However, Fe^{3+} has a larger mass than Mg^{2+}, which leads to decreased wavenumbers in the Raman spectra. The positions of the high wavenumber peak of the Raman ν_1 mode are almost the same in magnesiocopiapite (1019 cm^{-1}) and ferricopiapite (1019 cm^{-1}) resulting from the cancellation of the bond length effect and the mass effect. For the low wavenumber peak of the Raman ν_1 mode, the mass effect dominates, i.e. magnesiocopiapite (995 cm^{-1}) has a higher wavenumber peak than ferricopiapite (990 cm^{-1}). Substitutions in copiapite structures happen only in the I octahedra, and those I octahedra do not share oxygen with the $(SO_4)^{2-}$ tetrahedra. Therefore, the effect on the energy change of fundamental vibrational modes of $(SO_4)^{2-}$ due to cation substitution is not straightforward.

Mid-IR ATR spectral results

The mid-IR ATR spectra for different synthetic copiapite samples are very similar (Fig. 5). This similarity was also observed by Majzlan and Michallik.[41] A broad H_2O absorption band appears in the 2800–3600 cm^{-1} spectral range (Fig. 5(a)). This broad band was also reported by Majzlan and Michallik.[41] Adjacent to the broad band, a sharp $(OH)^-$ stretching peak appears for all copiapite samples, as marked by the dash line in Fig. 5(a).

The peak position of the water bending mode (1635 cm^{-1}) of all four synthetic copiapite samples in this study is quite similar to that reported by Majzlan and Michallik at 1637 cm^{-1} for copiapite-group minerals.[41] In a mid-IR emissivity study of ferricopiapite, however, the water bending mode was observed at 1649 and 1444 cm^{-1}.[63]

As indicated by the dashed line in Fig. 5(b), the ν_3 mode of $(SO_4)^{2-}$ appears as a strong peak at 1090–1095 cm^{-1}, a weak peak at 1209–1224 cm^{-1}, and two weak shoulders near 1033–1038 and

 Copyright © 2010 John Wiley & Sons, Ltd.

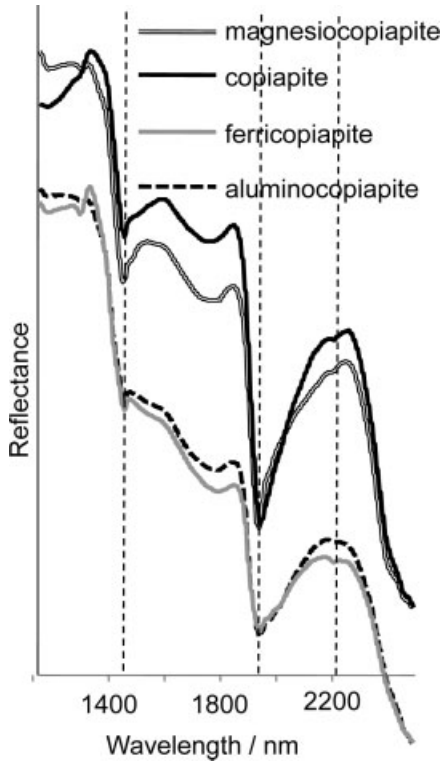

Figure 6. NIR reflectance spectra of the four copiapite samples. The spectra are vertically shifted in order to show the major differences between the spectra of trivalent copiapite samples from those of bivalent copiapite samples. Major H_2O bands and peak arising from a combination mode with OH are indicated by dash lines.

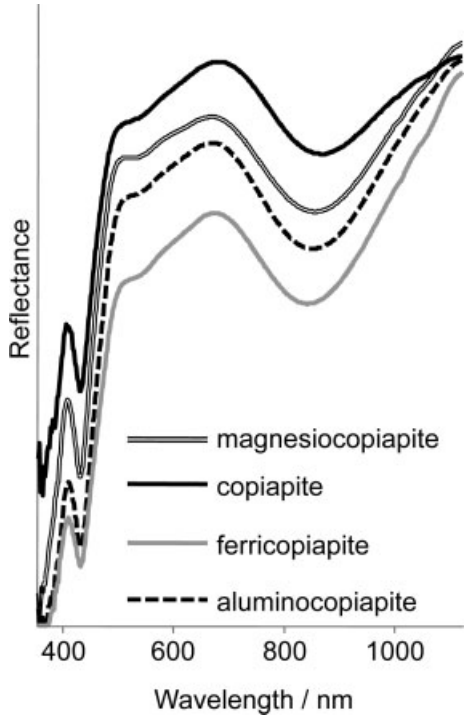

Figure 7. Vis–NIR reflectance spectra of four copiapite minerals. The spectra are vertically shifted in order to show the major differences among the spectra.

near 1174–1181 cm^{-1}. The mid-IR absorbance study by Majzlan and Michallik reported the ν_3 peak positions at 1061, 1081, 1135 and 1223 cm^{-1}.[41] The thermal emission spectra of ferricopiapite show ν_3 peaks at 1220, ~1116 and 1050 cm^{-1}.[63] A mid-IR reflection study of copiapite-group samples finds the ν_3 peaks at positions similar to that found in the thermal emission study.[64] The Raman active ν_1 peaks of isolated $(SO_4)^{2-}$ tetrahedra should be weak in the mid-IR spectra. However, for the four copiapite species in this study, the intensity of the ν_1 peak near 990 cm^{-1} is comparable to that of the strong ν_3 peak near 1090–1095 cm^{-1}. This strong ν_1 band showed up in the Raman spectra (Fig. 4(b)) and it was also observed in previous studies.[41,63,64] This weakening of the selection rules can be caused by the distortion of the $(SO_4)^{2-}$ tetrahedra due to their low site symmetries in the copiapite-group structures.

No obvious shifts in the peak position among copiapite species were observed in the mid-IR absorbance study.[41] However, the mid-IR diffuse reflection study showed position shifts for IR peaks among the copiapite species (1045–1060 cm^{-1} for ν_3 and 993–1011 cm^{-1} for ν_1).[64] We observed only subtle shifts in the peak position among our copiapite samples in the mid-IR spectra for both ν_3 (1090–1095 cm^{-1}) and ν_1 (987–993 cm^{-1}). The shift in the Raman ν_1 peak (1019–1026 cm^{-1}) caused by cation substitutions was not observed in the mid-IR spectra, as this peak was very weak.

The vis-NIR spectral results

The NIR spectra in the 1200–2500 nm spectral range of copiapite samples are shown in Fig. 6. Two prominent absorption bands appear near 1450 and near 1940 nm. Similar absorption bands of ferricopiapite were reported previously near the 6892 cm^{-1} (1450 nm) and near 5155 cm^{-1} (1940 nm).[65] These two prominent bands were also observed for copiapite-group samples by other studies.[64,66,67]

The 1940 nm (~5150 cm^{-1}) band should be a H_2O combinational mode ($\nu_3 + \nu_2$). The absorption band depth in the spectra of trivalent copiapite species is lower than that in the spectra of divalent copiapite species. The relatively shallow slope from 1940 to 2100 nm for trivalent copiapite species may be contributed by their two weak shoulders near 1976 and near 2012 nm. Magnesiocopiapite has a weak shoulder at 1978 nm, which may cause the slope change near 1960 nm. Bishop *et al*. reported two additional peaks (1980 nm for iron-rich copiapite and 2010 nm for aluminum-rich copiapite).[64] Frost *et al*. also observed a band at 4974 cm^{-1} (2010 nm).[65] An NIR reflectance spectroscopy study of sulfate minerals showed that the spectral slope for one of the copiapite samples is higher than that of ferricopiapite samples in the 1940–2100 nm spectral range.[66] Our results are consistent with these previous studies.

The absorption band centered near 1450 nm (6900 cm^{-1}) is the H_2O combinational mode ($\nu_3 + 2\nu_2$), and similar assignments have been made by Cloutis *et al*. and Shama *et al*.[54,66] Unlike the sharp band at 1360 nm in the copiapite spectrum reported by Cloutis *et al*.,[66] the sharp peak on top of the 1450-nm broad continuous absorption band might be coming from the combination of ν_3 from H_2O and the OH stretching (Fig. 6).

A weak band appears near 2210 nm (4525 cm^{-1}) for each of our copiapite samples, and this band was also observed by Bishop *et al*.[64] This band may be assigned to the combination of the OH stretching mode (~3520 cm^{-1}) with the sulfate stretching mode (~1000 cm^{-1}).

Three prominent Fe^{3+} electronic absorption features occur in the 400–1100 nm vis–NIR spectral range (Fig. 7). These

Copyright © 2010 John Wiley & Sons, Ltd.

spin-forbidden transitions are due to the Fe–OH–Fe linked structure.[46] A sharp band due to the $^6A_{1g} \rightarrow (^4A_{1g}, {}^4E_g)$ transition appears at 430 nm for all four copiapite species, a shoulder near 530 nm is caused by the $^6A_{1g} \rightarrow {}^4T_{2g}$ transition and the following broad band is caused by the $^6A_{1g} \rightarrow {}^4T_{1g}$ transition.[68,69] The broad band occurs at 854 nm for our magnesiocopiapite sample (855 nm was reported by Rossman[46]), at 850 nm for ferricopiapite, at 853 nm for aluminocopiapite and at 866 nm for copiapite (i.e. at a longer wavelength than other three samples).

In a previous vis–NIR reflectance spectroscopic study of copiapite-group samples,[64] no apparent band position differences were observed among ferric, Al and Mg copiapite species. Another vis–NIR reflectance spectroscopic study suggests the existence of electronic transition of Fe^{2+} near 900 nm for copiapite.[66] We believe that this ferrous spectral feature may have merged with the 850-nm Fe^{3+} transition band in copiapite spectrum, causing the band center to shift to longer wavelength, as demonstrated in Fig. 7.

Application to Mars

Based on the ubiquitous occurrence of sulfates at Mars subsurface and in outcrops, there must have been a time period in Mars's history when large amount of sulfur was available. At some locations with limited amount of water, the pH value of the SO_4-bearing aqueous solution could have been relatively low. A variety of cations (e.g. Mg, Fe, Ca and Al) might have been released into these solutions from the alterations of igneous rocks.

The alteration of Martian igneous rocks was observed by Spirit rover at Gusev with a wide range in the degree of alterations. A moderate olivine dissolution was identified within the Gusev plains' basalts[70] and a high degree of alteration was indicated by the elevated Fe^{3+}/Fe_{total} values (max. ~0.9) of the investigated rocks in the regions of Columbia Hills and Home Plate.[35] Although no direct evidence on the dissolution of pyroxene and feldspar was found by current Spirit investigation,[26,30,31] the compositional characters of some rocks do suggest the existences of phyllosilicates.[71,72] These phyllosilicates can come from the devitrification (or dissolution and recrystallization) of volcanic glasses.[73] Among these alterations, magnesium and iron are the major cations to be released from olivine,[74,75] with zinc and nickel as minor or trace constituents that are released together. Calcium, aluminum, sodium and potassium can be released into aqueous solutions from the alteration of volcanic glasses. When copiapite minerals precipitated from S-bearing aqueous solutions, Fe, Mg, Al, Zn Ni can enter the copiapite structure to form a variety of copiapite-group minerals on Mars. The dehydration or chemical alteration of copiapite minerals will produce other ferric sulfates with a lower hydration state Fe-hydroxide and Fe-oxides as observed on Mars.

The XRD instrument (CheMin) and the LIBS spectrometer (CamChem) on board the Mars Science Laboratory (MSL) will be sent to Mars in 2011. A Raman spectrometer will be carried by the ExoMars rover (2018). Mid-IR thermal emission spectrometers (TES, MiniTES) have been sent to Mars on orbiters (Mars Global Survey) and on MERs. Vis–NIR spectrometers of various spectral ranges were used on orbiters (OMEGA on Mars Express and CRISM on Mars Reconnaissance Orbiter) and on rovers and lander (Pancam of Spirit and Opportunity rovers and SSI on Phoenix lander).

The XRD and spectroscopic characterizations (Raman, LIBS, Mid-IR, vis–NIR) of four synthetic copiapite samples with cation substitutions made in this study provide a set of reference data for the identification and characterization of copiapite-group minerals on Mars. In the powder XRD patterns of four copiapite species, the three most intense lines showed a systematic 2θ change with cation substitution, and this change can be used to distinguish between different potential copiapite minerals in the MSL mission. The chemical compositions indicated by the LIBS study are consistent with those of ideal copiapite minerals. Further LIBS investigation under Martian conditions (namely 7 mbar CO_2 and subzero temperatures) will be performed on these four samples to provide reference LIBS spectra, which might help finding potential copiapite minerals on Mars through the MSL mission. A systematic Raman peak shift of the $(SO_4)^{2-}$ ν_1 mode was caused by cation substitution. This systematic shift of Raman peaks serves to distinguish between different copiapite minerals using the data acquired from the Raman instrument on board the ExoMars mission. Strong ν_1 peaks appear in the mid-IR spectra, indicating a weakening of selection rules due to the low site symmetry of the $(SO_4)^{2-}$ tetrahedra in copiapite-group structures. Two additional NIR peaks near 1976 and 2012 nm of trivalent copiapite species makes the spectral slope of trivalent copiapite species in the 1940–2100 nm range shallower than that of the divalent copiapite species. The difference between ferrous copiapite and the other three copiapite species for the 850-nm electronic band suggests that the electronic transition band of Fe^{2+} near 900 nm shifted the Fe^{3+} 850-nm band center of copiapite to a longer wavelength (866 nm).

Acknowledgements

Janice Bishop gave much guidance for this work. Thanks are due for all the referee's constructive reviews. This study was supported partially by the Chinese Scholarship Council (to WGK) and partially by a NASA Mars Fundamental Research project (NNX07AQ34G).

References

[1] K. A. Hudson-Edwards, C. Schell, M. G. Macklin, *Appl. Geochem.* **1999**, *14*, 1015.
[2] T. Buckby, S. Black, M. L. Coleman, M. E. Hodson, *Mineral. Mag.* **2003**, *67*, 263.
[3] P. Sobron, A. Sanz, T. Acosta, F. Rull, *Spectrochim. Acta A* **2009**, *71*, 1678.
[4] C. A. Cravotta, *Am. Chem. Soc.* **1994**, *550*, 345.
[5] D. K. Nordstrom, C. N. Alpers, *Natl. Acad. Sci.* **1999**, *96*, 3455.
[6] H. E. Jamieson, C. Robinson, C. N. Alpers, R. B. McCleskey, D. K. Nordstrom, R. C. Peterson, *Chem. Geol.* **2005**, *215*, 387.
[7] R. E. Arvidson, F. Poulet, J. P. Bibring, M. Wolff, A. Gendrin, R. V. Morris, J. J. Freeman, Y. Langevin, N. Mangold, G. Bellucci, *Science* **2005**, *307*, 1591.
[8] J. P. Bibring, Y. Langevin, A. Gendrin, B. Gondet, F. Poulet, M. Berthe, A. Soufflot, R. Arvidson, N. Mangold, J. Mustard, P. Drossart, O. Team, *Science* **2005**, *307*, 1576.
[9] A. Gendrin, N. Mangold, J. P. Bibring, Y. Langevin, B. Gondet, F. Poulet, G. Bonello, C. Quantin, J. Mustard, R. Arvidson, S. LeMouélic, *Science* **2005**, *307*, 158.
[10] Y. Langevin, F. Poulet, J. P. Bibring, B. Gondet, *Science* **2005**, *307*, 1584.
[11] K. A. Lichtenberg, R. E. Arvidson, R. V. Morris, S. L. Murchie, J. L. Bishop, T. D. Glotch, E. Noe Dobrea, J. F. Mustard, J. Andrews-Hanna, L. H. Roach, The CRISM Team, *J. Geophys. Res.* **2010**, *115*, E00D17.
[12] S. Murchie, R. Arvidson, P. Bedini, K. Beisser, J. P. Bibring, J. Bishop, J. Boldt, P. Cavender, T. Choo, R. T. Clancy, E. H. Darlington, D. D. Marais, R. Espiritu, D. Fort, R. Green, E. Guinness, J. Hayes, C. Hash, K. Heffernan, J. Hemmler, G. Heyler, D. Humm, J. Hutcheson, N. Izenberg, R. Lee, J. Lees, D. Lohr, E. Malaret,

Copyright © 2010 John Wiley & Sons, Ltd.

T. Martin, J. A. McGovern, P. McGuire, R. Morris, J. Mustard, S. Pelkey, E. Rhodes, M. Robinson, T. Roush, E. Schaefer, G. Seagrave, F. Seelos, P. Silverglate, S. Slavney, M. Smith, W. J. Shyong, K. Strohbehn, H. Taylor, P. Thompson, B. Tossman, M. Wirzburger, M. Wolff, *J. Geophys. Res. Planets* **2007**, *112*, E05S03.

[13] S. Murchie, L. Roach, F. Seelos, R. Milliken, J. Mustard, R. Arvidson, S. Wiseman, K. Lichtenberg, J. Andrews-Hanna, J. Bishop, J. P. Bibring, M. Parente, R. Morris, *J. Geophys. Res. Planets* **2009**, *114*, E11009.

[14] S. L. Murchie, J. F. Mustard, B. L. Ehlmann, R. E. Milliken, J. L. Bishop, N. K. McKeown, E. Z. N. Dobrea, F. P. Seelos, D. L. Buczkowski, S. M. Wiseman, R. E. Arvidson, J. J. Wray, G. Swayze, R. N. Clark, D. J. D. Marais, A. S. McEwen, J. P. Bibring, *J. Geophys. Res. Planets* **2009**, *114*, E00D06.

[15] L. H. Roach, J. F. Mustard, S. L. Murchie, J. P. Bibring, F. Forget, K. W. Lewis, O. Aharonson, M. Vincendon, J. L. Bishop, *J. Geophys. Res. Planets* **2009**, *114*, E00D02.

[16] L. H. Roach, J. F. Mustard, G. Swayze, R. E. Milliken, J. L. Bishop, S. L. Murchie, K. Lichtenberg, *Icarus* **2010**, *206*, 253.

[17] L. H. Roach, J. F. Mustard, M. D. Lane, J. L. Bishop, *Icarus* **2010**, *207*, 659.

[18] S. M. Wiseman, R. E. Arvidson, J. C. Andrews-Hanna, R. N. Clark, N. L. Lanza, D. D. Marais, G. A. Marzo, R. V. Morris, S. L. Murchie, H. E. Newsom, E. Z. N. Dobrea, A. M. Ollila, F. Poulet, T. L. Roush, F. P. Seelos, G. A. Swayze, *Geophys. Res. Lett.* **2008**, *35*, 19.

[19] S. M. Wiseman, R. E. Arvidson, R. V. Morris, F. Poulet, J. C. Andrews Hanna, J. L. Bishop, S. L. Murchie, F. P. Seelos, D. Des Marais, J. L. Griffes, *J. Geophys. Res.* **2010**, *115*, E00D18.

[20] L. H. Roach, J. F. Mustard, S. L. Murchie, J. L. Bishop, C. M. Weitz, A. T. Knudson, J. P. Bibring, S. M. Pelkey, B. L. Ehlmann, The CRISM Science Team, *Seventh International Conference on Mars*, 9–13 July 2007, http://www.lpi.usra.edu/meetings/7thmars2007/pdf/3223.pdf, **2007**, 3223.

[21] R. E. Milliken, G. A. Swayze, R. E. Arvidson, J. L. Bishop, R. N. Clark, B. L. Ehlmann, R. O. Green, J. P. Grotzinger, R. V. Morris, S. L. Murchie, J. F. Mustard, C. Weitz, *Geology* **2008**, *36*, 847.

[22] J. L. Bishop, M. Parente, C. M. Weitz, E. Z. N. Dobrea, L. H. Roach, S. L. Murchie, P. C. McGuire, N. K. McKeown, C. M. Rossi, A. J. Brown, W. M. Calvin, R. Milliken, J. F. Mustard, *J. Geophys. Res. Planets* **2009**, *114*, E00D09.

[23] R. E. Arvidson, S. W. Squyres, R. C. Anderson, J. F. Bell, D. Blaney, J. Bruckner, N. A. Cabrol, W. M. Calvin, M. H. Carr, P. R. Christensen, B. C. Clark, L. Crumpler, D. J. Des Marais, P. A. de Souza, C. d'Uston, T. Economou, J. Farmer, W. H. Farrand, W. Folkner, M. Golombek, S. Gorevan, J. A. Grant, R. Greeley, J. Grotzinger, E. Guinness, B. C. Hahn, L. Haskin, K. E. Herkenhoff, J. A. Hurowitz, S. Hviid, J. R. Johnson, G. Klingelhöfer, A. H. Knoll, G. Landis, C. Leff, M. Lemmon, R. Li, M. B. Madsen, M. C. Malin, S. M. McLennan, H. Y. McSween, D. W. Ming, J. Moersch, R. V. Morris, T. Parker, J. W. Rice, L. Richter, R. Rieder, D. S. Rodionov, C. Schroder, M. Sims, M. Smith, P. Smith, L. A. Soderblom, R. Sullivan, S. D. Thompson, N. J. Tosca, A. Wang, H. Wanke, J. Ward, T. Wdowiak, M. Wolff, A. Yen, *J. Geophys. Res. Planets* **2006**, *111*, E02S01.

[24] R. E. Arvidson, S. W. Ruff, R. V. Morris, D. W. Ming, L. S. Crumpler, A. S. Yen, S. W. Squyres, R. J. Sullivan, J. F. Bell, N. A. Cabrol, B. C. Clark, W. H. Farrand, R. Gellert, R. Greenberger, J. A. Grant, E. A. Guinness, K. E. Herkenhoff, J. A. Hurowitz, J. R. Johnson, G. Klingelhöfer, K. W. Lewis, R. Li, T. J. McCoy, J. Moersch, H. Y. McSween, S. L. Murchie, M. Schmidt, C. Schroder, A. Wang, S. Wiseman, M. B. Madsen, W. Goetz, S. M. McLennan, *J. Geophys. Res. Planets* **2008**, *113*, E12S33.

[25] S. W. Squyres, R. E. Arvidson, J. F. Bell, J. Bruckner, N. A. Cabrol, W. Calvin, M. H. Carr, P. R. Christensen, B. C. Clark, L. Crumpter, D. J. Des Marais, C. d'Uston, T. Economou, J. Farmer, W. Farrand, W. Folkner, M. Golombek, S. Gorevan, J. A. Grant, R. Greeley, J. Grotzinger, L. Haskin, K. E. Herkenhoff, S. Hviid, J. Johnson, G. Klingelhöfer, A. H. Knoll, G. Landis, M. Lemmon, R. Li, M. B. Madsen, M. C. Malin, S. M. McLennan, H. Y. McSween, D. W. Ming, J. Moersch, R. V. Morris, T. Parker, J. W. Rice, L. Richter, R. Rieder, M. Sims, M. Smith, P. Smith, L. A. Soderblom, R. Sutlivan, H. Wanke, T. Wdowiak, M. Wolff, A. Yen, *Science* **2004**, *306*, 1698.

[26] S. W. Squyres, R. E. Arvidson, D. Bollen, J. F. Bell, J. Bruckner, N. A. Cabrol, W. M. Calvin, M. H. Carr, P. R. Christensen, B. C. Clark, L. Crumpler, D. J. Des Marais, C. d'Uston, T. Economou, J. Farmer, W. H. Farrand, W. Folkner, R. Gellert, T. D. Glotch, M. Golombek, S. Gorevan, J. A. Grant, R. Greeley, J. Grotzinger, K. E. Herkenhoff, S. Hviid, J. R. Johnson, G. Klingelhöfer, A. H. Knoll, G. Landis, M. Lemmon, R. Li, M. B. Madsen, M. C. Malin, S. M. McLennan, H. Y. McSween, D. W. Ming, J. Moersch, R. V. Morris, T. Parker, J. W. Rice, L. Richter, R. Rieder, C. Schroder, M. Sims, M. Smith, P. Smith, L. A. Soderblom, R. Sullivan, N. J. Tosca, H. Wanke, T. Wdowiak, M. Wolff, A. Yen, *J. Geophys. Res. Planets* **2006**, *111*, E12S12.

[27] G. Klingelhöfer, R. V. Morris, B. Bernhardt, C. Schroder, D. S. Rodionov, P. A. de Souza, A. Yen, R. Gellert, E. N. Evlanov, B. Zubkov, J. Foh, U. Bonnes, E. Kankeleit, P. Gutlich, D. W. Ming, F. Renz, T. Wdowiak, S. W. Squyres, R. E. Arvidson, *Science* **2004**, *306*, 1740.

[28] B. C. Clark, R. V. Morris, S. M. McLennan, R. Gellert, B. Jolliff, A. H. Knoll, S. W. Squyres, T. K. Lowenstein, D. W. Ming, N. J. Tosca, A. Yen, P. R. Christensen, S. Gorevan, J. Bruckner, W. Calvin, G. Dreibus, W. Farrand, G. Klingelhöfer, H. Waenke, J. Zipfel, J. F. Bell, J. Grotzinger, H. Y. McSween, R. Rieder, *Earth Planet. Sci. Lett.* **2005**, *240*, 73.

[29] R. Gellert, R. Rieder, J. Bruckner, B. C. Clark, G. Dreibus, G. Klingelhöfer, G. Lugmair, D. W. Ming, H. Wanke, A. Yen, J. Zipfel, S. W. Squyres, *J. Geophys. Res. Planets* **2006**, *111*, E02S05.

[30] D. W. Ming, D. W. Mittlefehldt, R. V. Morris, D. C. Golden, R. Gellert, A. Yen, B. C. Clark, S. W. Squyres, W. H. Farrand, S. W. Ruff, R. E. Arvidson, G. Klingelhöfer, H. Y. McSween, D. S. Rodionov, C. Schroder, P. A. de Souza, A. Wang, *J. Geophys. Res. Planets* **2006**, *111*, E02S12.

[31] D. W. Ming, R. Gellert, R. V. Morris, R. E. Arvidson, J. Brückner, B. C. Clark, B. A. Cohen, C. d'Uston, T. Economou, I. Fleischer, G. Klingelhöfer, T. J. McCoy, D. W. Mittlefehldt, M. E. Schmidt, C. Schroder, S. W. Squyres, E. Treguier, A. S. Yen, J. Zipfel, *J. Geophys. Res. Planets* **2008**, *113*, E12S39.

[32] S. W. Ruff, P. R. Christensen, D. L. Blaney, W. H. Farrand, J. R. Johnson, J. R. Michalski, J. E. Moersch, S. P. Wright, S. W. Squyres, *J. Geophys. Res. Planets* **2006**, *111*, E12S18.

[33] A. Wang, J. F. Bell, R. Li, J. R. Johnson, W. H. Farrand, E. A. Cloutis, R. E. Arvidson, L. Crumpler, S. W. Squyres, S. M. McLennan, K. E. Herkenhoff, S. W. Ruff, A. T. Knudson, W. Chen, R. Greenberger, *J. Geophys. Res. Planets* **2008**, *113*, E12S40.

[34] A. S. Yen, R. V. Morris, B. C. Clark, R. Gellert, A. T. Knudson, S. Squyres, D. W. Mittlefehldt, D. W. Ming, R. Arvidson, T. Mccoy, M. Schmidt, J. Hurowitz, R. Li, J. R. Johnson, *J. Geophys. Res. Planets* **2008**, *113*, E06S10.

[35] R. V. Morris, G. Klingelhöfer, C. Schroder, D. S. Rodionov, A. Yen, D. W. Ming, P. A. de Souza, I. Fleischer, T. Wdowiak, R. Gellert, B. Bernhardt, E. N. Evlanov, B. Zubkov, J. Foh, U. Bonnes, E. Kankeleit, P. Gutlich, F. Renz, S. W. Squyres, R. E. Arvidson, *J. Geophys. Res. Planets* **2006**, *111*, E02S13.

[36] R. V. Morris, G. Klingelhöfer, C. Schroder, I. Fleischer, D. W. Ming, A. S. Yen, R. Gellert, R. E. Arvidson, D. S. Rodionov, L. S. Crumpler, B. C. Clark, B. A. Cohen, T. J. McCoy, D. W. Mittlefehldt, M. E. Schmidt, P. A. de Souza, S. W. Squyres, *J. Geophys. Res. Planets* **2008**, *113*, E12S42.

[37] J. R. Johnson, J. F. Bell, E. Cloutis, M. Staid, W. H. Farrand, T. McCoy, M. Rice, A. Wang, A. Yen, *Geophys. Res. Lett.* **2007**, *34*, 202.

[38] M. D. Lane, J. L. Bishop, M. D. Dyar, P. L. King, M. Parente, B. C. Hyde, *Am. Miner.* **2008**, *93*, 728.

[39] M. Parente, J. L. Bishop, J. F. Bell, *Icarus* **2009**, *203*, 42.

[40] L. R. Friedlander, N. J. Tosca, R. E. Arvidson, *Lunar and Planetary Science Conference XXVIII*, 12–16 March 2007, http://www.lpi.usra.edu/meetings/lpsc2007/pdf/2049.pdf, **2007**, 2049.

[41] J. Majzlan, R. Michallik, *Mineral. Mag.* **2007**, *71*, 553.

[42] J. Majzlan, B. Kiefer, *Can. Mineral.* **2006**, *44*, 1227.

[43] L. Fanfani, A. Nunzi, P. F. Zana zzi, A. R. Zanzari, *Am. Mineral.* **1973**, *58*, 314.

[44] W. G. Fateley, N. T. McDevitt, F. F. Bently, *Appl. Spectrosc.* **1971**, *25*, 155.

[45] G. R. Rossman, *Rev. Mineral.* **1988**, *18*, 207.

[46] G. R. Rossman, *Am. Mineral.* **1975**, *60*, 698.

[47] J. L. Bishop, E. Murad, *Am. Mineral.* **2005**, *90*, 1100.

[48] P. SÜSSE, *Z. Kristallogr.* **1972**, *135*, 34.

[49] B. Salle, J. L. Lacour, E. Vors, P. Fichet, S. Maurice, D. A. Cremers, R. C. Wiens, *Spectrochim. Acta B* **2004**, *59*, 1413.

[50] L. Dudragne, P. Adam, J. Amouroux, *Appl. Spectrosc.* **1998**, *52*, 1321.

Copyright © 2010 John Wiley & Sons, Ltd.

[51] P. Sobron, C. N. Alpers, A. Wang, *Lunar and Planetary Science Conference XLI*, 1–5 March 2010, http://www.lpi.usra.edu/meetings/lpsc2010/pdf/2585.pdf, **2010**, 2585.
[52] B. Salle, J.-L. Lacour, E. Vors, P. Fichet, S. Maurice, D. A. Cremers, R. C. Wiens, *Spectrochim. Acta B* **2004**, *59*, 1413.
[53] J. J. Perkins, S. K. Sharma, S. M. Clegg, A. K. Misra, R. C. Wiens, J. E. Barefied, *Lunar and Planetary Science Conference XL*, 23–27 March 2009, http://www.lpi.usra.edu/meetings/lpsc2009/pdf/1397.pdf, **2009**, 1397.
[54] S. K. Sharma, A. K. Misra, P. G. Lucey, R. C. Wiens, S. M. Clegg, *Spectrochim. Acta A* **2007**, *68*, 1036.
[55] C. H. Chio, S. K. Sharma, D. W. Muenow, *Spectrochim. Acta A* **2005**, *61*, 2428.
[56] C. P. Chio, S. K. Sharma, D. W. Muenow, *J. Raman Spectrosc.* **2007**, *38*, 87.
[57] A. Wang, B. L. Jolliff, L. A. Haskin, K. E. Kuebler, K. M. Viskupic, *Am. Mineral.* **2001**, *86*, 790.
[58] K. E. Kuebler, B. L. Jolliff, A. Wang, L. A. Haskin, *Geochim. Cosmochim. Acta* **2006**, *70*, 6201.
[59] R. G. Herman, C. E. Bogdan, A. J. Sommer, D. R. Simpson, *Appl. Spectrosc.* **1987**, *41*, 437.
[60] K. E. Kuebler, A. Wang, K. Abbott, L. A. Haskin, *Lunar and Planetary Science Conference XXXII*, 12–16 March 2001, http://www.lpi.usra.edu/meetings/lpsc2001/pdf/1889.pdf, **2001**, 1889.
[61] A. Wang, K. Kuebler, B. Jolliff, L. A. Haskin, *J. Raman Spectrosc.* **2004**, *35*, 504.
[62] J. J. Freeman, A. Wang, K. E. Kuebler, B. L. Jolliff, L. A. Haskin, *Can. Mineral.* **2008**, *46*, 1477.
[63] M. D. Lane, *Am. Mineral.* **2007**, *92*, 1.
[64] J. L. Bishop, M. D. Dyar, J. Majzlan, M. D. Lane, *Lunar and Planetary Science Conference XL*, 23–27 March 2009, http://www.lpi.usra.edu/meetings/lpsc2009/pdf/2073.pdf, **2009**, 2073.
[65] R. L. Frost, R. A. Wills, W. Martens, M. Weier, B. J. Reddy, *Spectrochim. Acta A* **2005**, *62*, 42.
[66] E. A. Cloutis, F. C. Hawthorne, S. A. Mertzman, K. Krenn, M. A. Craig, D. Marcino, M. Methot, J. Strong, J. F. Mustard, D. L. Blaney, J. F. Bell, F. Vilas, *Icarus* **2006**, *184*, 121.
[67] M. D. Dyar, J. F. Holden, J. L. Bishop, M. D. Lane, *Lunar and Planetary Science Conference XL*, 23–27 March 2009, http://www.lpi.usra.edu/meetings/lpsc2009/pdf/2221.pdf, **2009**, 2221.
[68] R. G. Burns, *Mineralogical Applications of Crystal Field Theory* (2nd edn), Cambridge University Press: London, **1993**, pp 24.
[69] J. K. Crowley, D. E. Williams, J. M. Hammarstrom, N. Piatak, I.-M. Chou, J. C. Mars, *Geochem. Explor. Environ. Anal.* **2003**, *3*, 219.
[70] J. A. Hurowitz, S. M. McLennan, N. J. Tosca, R. E. Arvidson, J. R. Michalski, D. W. Ming, C. Schroder, S. W. Squyres, *J. Geophys. Res. Planets* **2006**, *111*, E02S19.
[71] A. Wang, L. A. Haskin, S. W. Squyres, B. L. Jolliff, L. Crumpler, R. Gellert, C. Schroder, K. Herkenhoff, J. Hurowitz, N. J. Tosca, W. H. Farrand, R. Anderson, A. T. Knudson, *J. Geophys. Res. Planets* **2006**, *111*, E02S16.
[72] B. C. Clark, R. E. Arvidson, R. Gellert, R. V. Morris, D. W. Ming, L. Richter, S. W. Ruff, J. R. Michalski, W. H. Farrand, A. Yen, K. E. Herkenhoff, R. Li, S. W. Squyres, C. Schroder, G. Klingelhöfer, J. F. Bell, *J. Geophys. Res. Planets* **2007**, *112*, E06S01.
[73] J. L. Gooding, *Icarus* **1978**, *33*, 485.
[74] R. A. Eggleton, *Rates of Chemical Weathering of Rocks and Minerals.* (Eds.:S. M. Colman, D. P. Dethier), Academic Press: Florida, **1986**, pp 21.
[75] N. J. Tosca, S. M. McLennan, D. H. Lindsley, M. A. A. Schoonen, *J. Geophys. Res. Planets* **2004**, *109*, E05003.

Copyright © 2010 John Wiley & Sons, Ltd.